Atmos. Chem. Phys. Discuss., https://doi.org/10.5194/acp-2018-1266
Manuscript under review for journal Atmos. Chem. Phys.
Discussion started: 2 January 2019

Atmospheric Chemistry and Physics Discussions

MAX-DOAS measurements of tropospheric NO_2 and HCHO in Nanjing and the comparison to OMI observations

Ka Lok Chan[1], Zhuoru Wang[1], Aijun Ding[2], Klaus-Peter Heue[1], Yicheng Shen[2], Jing Wang[3], Feng Zhang[4], Nan Hao[5], and Mark Wenig[6]

[1]Remote Sensing Technology Institute (IMF), German Aerospace Center (DLR), Oberpfaffenhofen, Germany
[2]School of Atmospheric Sciences, Nanjing University, Nanjing, China
[3]Key Laboratory for Aerosol-Cloud-Precipitation of China Meteorological Administration, Nanjing University of Information Science and Technology, Nanjing, China
[4]Key Laboratory of Meteorological Disaster, Ministry of Education, Nanjing University of Information Science and Technology, Nanjing, China
[5]European Organisation for the Exploitation of Meteorological Satellites (EUMETSAT), Darmstadt, Germany
[6]Meteorological Institute, Ludwig-Maximilians-Universität München, München, Germany

Correspondence: Ka Lok Chan (ka.chan@dlr.de)

Abstract.

In this paper, we present long term observations of atmospheric nitrogen dioxide (NO_2) and formaldehyde (HCHO) in Nanjing using a Multi-AXis Differential Optical Absorption Spectroscopy (MAX-DOAS) instrument. Ground based MAX-DOAS measurements were performed from April 2013 to February 2017. The MAX-DOAS measurements of NO_2 and HCHO vertical column densities (VCDs) are used to validate OMI satellite observations over Nanjing. The comparison shows that the OMI observations of NO_2 correlate well with the MAX-DOAS data with Pearson correlation coefficient (R) of 0.91. However, OMI observations are on average a factor of 3 lower than the MAX-DOAS measurements. Replacing the a priori NO_2 profiles by the MAX-DOAS profiles in the OMI NO_2 VCD retrieval would increase the OMI NO_2 VCDs by ∼30 % with correlation nearly unchanged. The comparison result of MAX-DOAS and OMI observations of HCHO VCD shows a good agreement with R of 0.75 and the slope of the regression line is 0.99. We developed a new technique to assemble the source contribution map using backward trajectory analysis. The age weighted backward propagation approach is applied to the MAX-DOAS measurements of NO_2 and HCHO to reconstruct the spatial distribution of NO_2 and HCHO over the Yangtze River Delta during summer and winter time. The reconstructed NO_2 fields show a distinct agreement with OMI satellite observations. However, due to the short atmospheric lifetime of HCHO, the backward propagated HCHO data does not show a strong spatial correlation with the OMI HCHO observations. The result shows the MAX-DOAS measurements are sensitive to the air pollution transportation in the Yangtze River Delta, indicating the air quality in Nanjing is significantly influenced by regional transportation of air pollutants. The MAX-DOAS data are also used to evaluate the effectiveness of air pollution control measures implemented during the Youth Olympic Games 2014. The MAX-DOAS data show a significant reduction of ambient aerosol, NO_2 and HCHO (30 % - 50 %) during the Youth Olympic Games. Our results provide a better understanding of the transportation and sources of pollutants in over the Yangtze River Delta as well as the effect of emission control measures during large international event, which are important for the future design of air pollution control policies.

Atmos. Chem. Phys. Discuss., https://doi.org/10.5194/acp-2018-1266
Manuscript under review for journal Atmos. Chem. Phys.
Discussion started: 2 January 2019

1 Introduction

Nitrogen dioxide (NO_2) and formaldehyde (HCHO) are major atmospheric pollutants playing crucial roles in atmospheric chemistry. NO_2 is a catalyst for ozone (O_3) formation in the troposphere, while also participating in the catalytic destruction of stratospheric O_3 (Crutzen, 1970). Major NO_2 sources include fossil fuel combustion, biomass burning, lightning and oxidation of ammonia (Bond et al., 2001; Zhang et al., 2003). The emissions of NO_2 show a significant increasing trend in China due to the rapid industrialization and economy development in the last two decades (Zhang et al., 2007; van der A et al., 2008; Zhao et al., 2013), making it one of the most severe air pollution problems. HCHO is an intermediate product of the oxidation of almost all volatile organic compounds (VOCs). Therefore, it is widely used as an indicator of non methane volatile organic compounds (NMVOCs) (Fried et al., 2011). VOCs also have significant impacts on the abundance of hydroxyl (OH) radicals in the atmosphere, which is the major oxidant in the tropospheric. Major HCHO sources over the continents include the oxidation of VOCs emitted from plants, biomass burning, traffic and industrial emissions. Oxidation of methane (CH_4) emitted from the ocean is the main source of HCHO over water. Both NO_2 and HCHO contribute to the formation of secondary aerosols (Jang and Kamens, 2001) and they are toxic to human in high concentration. The spatial distribution of NO_2 and HCHO is strongly related to their emissions due to their short atmospheric lifetime. Consequently, it is important to understand the spatial and temporal variations of atmospheric NO_2 and HCHO for better air pollution management and control.

Multi-AXis Differential Optical Absorption Spectroscopy (MAX-DOAS) is a powerful remote sensing measurement technique which provides valuable vertical distribution information of atmospheric aerosols and trace gases (Platt and Stutz, 2008). Information of tropospheric aerosols and traces gases are obtained from the molecular absorption in the ultraviolet and visible spectral bands by applying the differential optical absorption spectroscopy (DOAS) technique to the observations of scattered sun light spectrum in several different viewing directions. As the experimental setup of MAX-DOAS is rather simple and inexpensive, it has been widely used for the observation of atmospheric aerosols and trace gases in the past decade (Hönninger and Platt, 2002; Hönninger et al., 2004; Wittrock et al., 2004; Frieß et al., 2006; Irie et al., 2008; Li et al., 2010; Clémer et al., 2010; Halla et al., 2011; Li et al., 2013; Ma et al., 2013; Chan et al., 2015; Jin et al., 2016; Wang et al., 2016; Chan et al., 2018). MAX-DOAS measurements are highly sensitive to aerosols and trace gases in the lower troposphere and provide valuable information of the vertical distribution of aerosol extinction and trace gases. The information of the aerosol and trace gas vertical profiles are particularly important for the study of the physical and chemical processes in the atmosphere.

Satellite based remote sensing measurements provide indispensable spatial information of air pollutants (Burrows et al., 1999; Bovensmann et al., 1999; Callies et al., 2000; Levelt et al., 2006). Trace gas columns are derived from the satellite observations of Earth's reflected solar spectrum for the investigation of atmospheric dynamics and emissions from both anthropogenic and natural sources (Beirle et al., 2003; Wenig et al., 2003; Beirle et al., 2004; Richter et al., 2005; Zhang et al., 2007; van der A et al., 2008). Satellite measurements can also be used to determine the effectiveness of emission control measures (Mijling et al., 2009; Witte et al., 2009; Wu et al., 2013; Chan et al., 2015). However, the uncertainties of satellite trace gas column retrieval are strongly dependent on the accuracy of the assumptions of trace gas vertical distributions. In addition, the temporal resolution of satellite measurements is often limited to single observation per day. Therefore, it is useful to compare

and integrate ground based and satellite observations for the interpretation of the spatial and temporal variation of NO_2 and HCHO.

Nanjing is the second largest city in the Yangtze River Delta and Eastern China. It is also the provincial capital of Jiangsu province. The population of Nanjing is about 8 million. Yangtze River is running through the city of Nanjing making it the largest inland port in China. Industrial, water and road transportation are the major anthropogenic sources of air pollutions in Nanjing. Due to its rapid development as well as its surrounding cities in the Yangtze River Delta, Nanjing is facing a series of air pollution problems in recent years. In addition, Nanjing has also hosted several important international events including the summer Youth Olympic Games in 2014. Therefore, it is important to have a better understanding of the air pollution sources in order to support the design of air quality related environmental policies in the future.

In this paper, we present long term MAX-DOAS observations of NO_2 and HCHO in Nanjing. Ground based MAX-DOAS measurements were performed from April 2013 to February 2017. Details of the MAX-DOAS experimental setup, the spectral analysis as well as the retrieval of the aerosol extinction, NO_2 and HCHO profiles are presented in section 2. Section 3.1 shows the validation of MAX-DOAS aerosol observations by comparing the reported aerosol optical depths (AODs) to sun photometer measurements. The comparison of NO_2 and HCHO VCDs measured by the MAX-DOAS and OMI satellite is presented in Section 3.2. An analysis of regional transport of pollutants over Yangtze River Delta is shown in section 3.4. In section 3.5, we presented an evaluation of the pollution reduction observed during the Youth Olympic Games in 2014.

2 Methodology

2.1 MAX-DOAS measurements

2.1.1 Experimental setup

A MAX-DOAS instrument was set up at a meteorological station of Nanjing University (32.12°N, 118.95°E) which is located on a small hill in the University campus at about 45 m above sea level. The meteorological station is located about 17 km northeast of the Nanjing city center and about 5 km south of the Yangtze River. The MAX-DOAS instrument for scattered sun-light measurements consists of a scanning telescope, a stepping motor controlling the viewing zenith angle of the telescope and a spectrometer. Scattered sun-light collected by the telescope is redirected by a quartz fiber to the spectrometer for spectral analysis. The field of view of the telescope is about 0.6°. An Ocean Optic USB2000 spectrometer equipped with a Sony ILX511 charge-coupled device (CCD) detector is used to cover the wavelength range from 288 nn to 434 nm. The full width half maximum (FWHM) spectral resolution of the spectrometer is 0.6 nm (at 360 nm).

A complete measurement cycle consists of scattered sun-light observations at elevation angle (α) of 1°, 2°, 3°, 6°, 10°, 18°, 30° and the zenith (90°). The viewing azimuth angle is adjusted to 320° (northwest). The exposure time and the number of scan of each measurement is adjusted automatically depending on the received intensity of the scattered sun-light spectrum in order to achieve a similar intensity level for all the measurements. A full measurement sequence takes about 5 - 10 minutes.

Atmos. Chem. Phys. Discuss., https://doi.org/10.5194/acp-2018-1266
Manuscript under review for journal Atmos. Chem. Phys.
Discussion started: 2 January 2019

Atmospheric Chemistry and Physics Discussions

2.1.2 Spectral retrieval

All the measurement spectra were first corrected for offset and dark current and then analyzed using the spectral analyzing software QDOAS (version 3.2). The MAX-DOAS spectral fit was performed at 2 different wavelength ranges for the retrieval of NO_2 and HCHO. In this study, the zenith spectrum ($\alpha = 90°$) is used as reference spectrum in the spectral analysis to retrieve the differential slant column densities (DSCDs). The differential slant column density (DSCD) is defined as the difference between the slant column density (SCD) of the measured spectrum and the corresponding zenith reference spectrum. The broad band spectral structures caused by Rayleigh and Mie scattering are removed by including a low order polynomial in the DOAS fit. Absorption cross section of several trace gases were included in the DOAS fit at different fitting ranges, details of the DOAS retrieval settings for each wavelength range are listed in Table 1. Small shift and squeeze of the wavelengths are allowed in the wavelength mapping process in order to compensate small uncertainties caused by the instability of the spectrograph.

Table 1. The DOAS retrieval settings for different wavelength bands.

Species	Temperature	Wavelength Range		Reference
		324.5 - 359 nm	338 - 370 nm	
BrO	223 K	✓	✓	Fleischmann et al. (2003)
HCHO	298 K	✓	✓	Meller and Moortgat (2000)
NO_2 [(a)]	298 K	✓	✓	Vandaele et al. (1998)
NO_2 [(a)]	220 K		✓	Vandaele et al. (1998)
O_3 [(b)]	223 K	✓	✓	Serdyuchenko et al. (2014)
O_3 [(b)]	243 K	✓	✓	Serdyuchenko et al. (2014)
O_4	293 K	✓	✓	Thalman and Volkamer (2013)
Ring		✓	✓	
Polynomial		5^{th} order	5^{th} order	

[(a)] I_0 correction is applied with SCD of 10^{17} molec/cm^2 (Aliwell et al., 2002).

[(b)] I_0 correction is applied with SCD of 10^{20} molec/cm^2 (Aliwell et al., 2002).

As clouds are not included in the radiative transfer calculation of the aerosol and trace gas profile retrieval, the retrieval result can be significantly influenced by the present of cloud in the atmosphere. Therefore, the retrieved DSCDs were first filtered by removing cloudy scenes before proceeding to the aerosol and trace gas profile retrieval. The vertical profile of the oxygen collision complex O_4 only varies in a small range with atmospheric pressure and temperature, the retrieved O_4 DSCDs and (relative) intensities are assumed to vary smoothly with time with the solar and viewing geometry. Rapid change of O_4 DSCDs and intensities indicates a sudden change in the radiative transport condition which is likely due to the present of clouds. Therefore, we applied a locally weighted regression smoothing filter (LOWESS) (Cleveland, 1981) with a regression window of 3 hours to the O_4 DSCDs and intensities time series at each elevation angle to filter data influenced by inhomogeneous and/or rapid changes of radiation transport conditions. Data with fast varying O_4 DSCDs and intensities were filter out. Only data with slow varying O_4 DSCDs and intensities were used in the aerosol and trace gas retrieval.

Atmos. Chem. Phys. Discuss., https://doi.org/10.5194/acp-2018-1266
Manuscript under review for journal Atmos. Chem. Phys.
Discussion started: 2 January 2019

Atmospheric Chemistry and Physics Discussions

2.1.3 Aerosol and trace gas profile retrieval

Previous studies show that there is a systematic discrepancy between observation and model simulation of O_4 DSCDs (Wagner et al., 2009; Clémer et al., 2010; Wagner et al., 2011; Chan et al., 2015; Wang et al., 2016; Chan et al., 2018; Zhang et al., 2018). A scaling correction factor has to be applied to the measured O_4 DSCDs in order to bring measurement and model results into agreement. However, the physical meaning of this observation is still not well understood (Ortega et al., 2016; Wagner et al., 2018). Theoretically, the optical path should be the longest under aerosol free condition for off zenith measurement. Thus, the MAX-DOAS measurement of O_4 DSCDs should be smaller than the one simulated with pure Rayleigh atmosphere. In this study, we compared the forward simulation of O_4 DSCDs under aerosol free condition to the O_4 DSCDs retrieved from the MAX-DOAS observations to examine the necessity of O_4 correction. Our result shows that the measured O_4 DSCDs occasionally exceeded the forward simulation results which implies that correction of O_4 DSCDs is necessary. The ratio between simulated and measured O_4 DSCD varies from 0.75 to 1.0 for cases where the measured O_4 DSCDs exceeded the forward simulation results. Our finding agrees with previous reported scaling correction factors of O_4 DSCDs which is ranging from 0.7 up to 1.0. In order to avoid over-correction due to the outliers, we take the 10th percentile instead of the minimum value of the simulated and measured O_4 DSCD ratio as the correction factor which is $\sim$0.8. All MAX-DOAS observations of O_4 DSCD are corrected by multiplying the correction factor of 0.8. From hereafter, all O_4 DSCDs are referring to the corrected O_4 DSCDs.

The conversion of the MAX-DOAS observations to aerosol extinction and trace gas profile requires inversion of the underlying radiative transfer equations. These equations cannot be linearized, therefore, it is suggested to fit the measurement quantities to the forward calculation of radiation transfer (Wagner et al., 2004; Hönninger et al., 2004; Sinreich et al., 2005; Frieß et al., 2006; Hartl and Wenig, 2013; Chan et al., 2018). As the vertical distribution profile of O_4 is very stable and it has several absorption bands in the ultraviolet and visible spectral range, it is commonly used as fitting quantity for the aerosols retrieval.

In this study, aerosol vertical profiles are retrieved at the 360 nm O_4 absorption band using the Munich Multiple wavelength MAX-DOAS retrieval algorithm (M^3) (Chan et al., 2018). The algorithm is developed based on the optimal estimation method (Rodgers, 2000) and utilizes the Library for Radiative Transfer (LibRadTran) model (Emde et al., 2016) as the forward model. A brief description of the aerosol and trace gases vertical profile retrieval algorithm and the parameterization used in this study are presented in the following. A more detailed description of the 3M retrieval algorithm can be found in Chan et al. (2018).

In this study, all valid MAX-DOAS observations within a single measurement cycle are grouped together for the aerosol vertical profile retrieval. Assuming the set of measurement can be reproduced by the forward model and the forward model results are dependent on the aerosol extinction profile, we can then retrieve the aerosol extinction profile by fitting the forward model results to the MAX-DOAS O_4 observations using the iterative Newton-Gauss method. As the information contained in the MAX-DOAS observations are most likely not enough to retrieve an unique aerosol extinction profile, we have to supply the necessary information to the aerosol inversion in a form of a priori aerosol profile. As the aerosol load in Nanjing varies in a wide range, using a fix a priori could result in over regularizing the retrieval under higher aerosol load conditions. Therefore,

we have implemented an iterative approach to avoid over regularizing the retrieval. We first use a fixed initial a priori to retrieve the aerosol extinction profile. The fixed a priori profile is then scaled to have the same aerosol optical depth retrieved from the previous run. Then the new a priori is used in the next run to retrieve the aerosol extinction profile. This procedure is repeated until the difference between the retrieved and a priori aerosol optical depth is less than 10 % or the number of iteration reaches the limit.

As aerosols are typically emitted and formed close to the surface in urban areas, we assume the a priori aerosol extinction profile follows an exponentially decreasing function with a scale height of 1.0 km. The aerosol optical depth (AOD) of the a priori aerosol profile is set to 0.5 for the retrieval at 360 nm. The uncertainties of the a priori aerosol profile are set to 100 % and the correlation length of the aerosol inversion is assumed to be 0.5 km. As MAX-DOAS measurements are more sensitive to the aerosol and trace gases close to the instrument, therefore, we divided the lowest 3.0 km of the troposphere into 15 layers with thickness of each layer of 200 m. A fix set of single scattering albedo of 0.92, asymmetry parameter of 0.68 and ground albedo of 0.04 is assumed in the radiative transfer calculations.

The aerosol information obtained from the procedure described above were used for the differential box air mass factor (ΔDAMF) calculation for the trace gas profile inversion. The ΔDAMFs were calculated at a single wavelength for the retrieval of trace gas profile using the radiative transfer model LibRadTran with the Monte Carlo simulation module MYSTIC (Emde et al., 2016). The ΔDAMF was assumed to be constant within the DOAS spectral fitting windows. In this study, vertical distribution profiles of NO_2 are retrieved at 360 nm. For HCHO vertical distribution profile retrieval, aerosol extinction profiles obtained at the 360 nm O_4 band are converted to 340 nm assuming a fixed Ångström coefficient (Ångström, 1929) of 1. The ΔDAMFs are subsequently calculated at 340 nm for the HCHO profile retrieval.

The atmosphere layer settings of the trace gas profile retrieval are the same as the one used in the aerosol profile retrieval. As the trace gas profile cannot be fully reconstructed by the small number of measurements, therefore, we use the optimal estimation method (Rodgers, 2000) with iterative approach to regularize the inversion (Chan et al., 2015, 2018). The first step uses a fixed initial a priori to retrieve the trace gas distribution. The fixed a priori profile is then scaled to have the vertical column retrieved from the first run. The scaled a priori is used in the next run to retrieve the trace gas profile. The process repeats until the difference between the retrieved and a priori trace gas vertical column is less than 10 % or the number of iteration reaches the limit. In this study, the a priori is assumed to follow an exponential decrease function with a scale height of 1.0 km. The uncertainty of the a priori profile is set to 100 % of the a priori and correlation length is set to 0.5 km in the trace gas profile inversion. The NO_2 vertical column density (VCD) of the a priori is set to 2×10^{16} molec/cm^2 while the a priori HCHO VCD is set to 1×10^{16} molec/cm^2.

2.2 Sun photometer measurements

A sun photometer was installed on the roof of a building of Nanjing University of Information Science and Technology (32.20°N, 118.70°E), which is located at the north bank of the Yangtze River. The sun photometer site is ~25 km northwest of the MAX-DOAS measurement site. The two instruments are separated by the Yangtze River. An industrial park is about 3 km east of the sun photometer site. Heavy industry factories, i.e., steel and cement plants are located in the industrial park.

In this study, AODs measured by the sun photometer were used for the inter-comparison study to validate the MAX-DOAS aerosol retrieval. Cloud screened data were used. The data consist of AOD measurements at 7 different wavelength channels from 340 nm to 1020 nm. AOD measurements at 340 nm and 380 nm are interpolated to 360 nm for comparison.

2.3 OMI Satellite observations

The Ozone Monitoring Instrument (OMI) is a passive nadir-viewing satellite borne imaging spectrometer (Levelt et al., 2006) on board the Earth Observing System's (EOS) Aura satellite. The instrument consists of two charge-coupled devices (CCDs) covering a wavelength range from 264 nm to 504 nm. A scan provides measurements at 60 positions across the orbital track covering a swath of approximately 2600 km. The spatial resolution of OMI varies from $\sim$320 km^2 (at nadir) to $\sim$6400 km^2 (at both edges of the swath). The instrument scans along 14.5 sun-synchronous polar orbits per day providing daily global coverage.

The NASA's OMI NO_2 and HCHO standard product version 3 (Krotkov et al., 2017; González Abad et al., 2015) are used in this study. In the NO_2 product, the slant column densities (SCDs) of NO_2 are derived from Earth's reflected spectra in the visible range (402 - 465 nm) using an iterative sequential algorithm (Marchenko et al., 2015). Previous studies show the updated SCDs are on average 10 - 40 % lower compared to the previous version of retrieval (Marchenko et al., 2015). The OMI NO_2 SCDs are converted to VCDs by using the concept of air mass factor (AMF) (Solomon et al., 1987). The AMFs are calculated using NO_2 profile simulated by the Global Modeling Initiative (GMI) chemistry transport model. The horizontal resolution of GMI is 1° (latitude) × 1.25° (longitude) (Rotman et al., 2001). Separation of stratospheric and tropospheric columns is achieved by the local analysis of the stratospheric field over unpolluted areas (Bucsela et al., 2013).

The OMI HCHO retrieval algorithm uses the direct fit of radiances in the spectral range from 328.5 nm to 356.5 nm for the SCD retrieval. In the current version of HCHO product, OMI radiance measurement over the remote Pacific is used as reference in the fitting process. This approach is reported to reduce the interferences from unresolved spectral structures in the retrieval of weak absorbers like HCHO (De Smedt et al., 2018). The retrieved SCDs are then converted to VCDs using the AMF approach. The AMFs are calculated based on climatological HCHO profiles.

2.4 Back trajectory modeling

The National Oceanic and Atmospheric Administration Air Resources Laboratory (NOAA ARL) developed HYbrid Single Particle Lagrangian Integrated Trajectory (HYSPLIT) model (Stein et al., 2015) (http://www.arl.noaa.gov/HYSPLIT.php) was used to investigate the transportation pollutants over Yangtze River Delta. Meteorological data from the Global Data Assimilation System (GDAS) with a spatial resolution of 0.5° × 0.5° and 24 vertical levels was used in the model for trajectory simulations. Backward trajectories are computed for air masses arriving at the mid point of each MAX-DOAS retrieval layer.

Atmos. Chem. Phys. Discuss., https://doi.org/10.5194/acp-2018-1266
Manuscript under review for journal Atmos. Chem. Phys.
Discussion started: 2 January 2019

3 Results and discussions

3.1 Compariosn of MAX-DOAS and sun photometer AODs

Aerosol optical depths (AODs) retrieved from the MAX-DOAS observations are compared to the sun photometer measurements. As the sampling resolution of the MAX-DOAS and the sun photometer are different, individual measurements are averaged to hourly, daily and monthly values for comparison. Figure 1 shows the scatter plot of AOD measured by the sun photometer and MAX-DOAS. Both datasets are cloud filtered. AODs measured by both MAX-DOAS and sun photometer are in general in good agreement. The Pearson correlation coefficient (R) of daily averaged data is 0.73. The slope of the total least squares regression between the two datasets is 0.56 with an offset of 0.13. The discrepancies between the two datasets can be explain by the difference of measurement technique and measurement location. The sun photometer derives AOD from direct sun measurements, while the MAX-DOAS retrieves AOD using the O_4 absorption information from scattered sun light. The sun photometer is sensitive to the entire column while the MAX-DOAS is mostly sensitive to aerosol at the lowest few kilometers of the troposphere. Therefore, the MAX-DOAS is likely to underestimate the AOD when there is an elevated aerosol layer in the upper troposphere. This explanation matches with the observations that the MAX-DOAS agrees better with the sun photometer under low aerosol conditions (AOD < 1) and underestimate the AOD during high AOD conditions. In addition, the MAX-DOAS and sun photometer are separated by a distance of $\sim$25 km and the sun photometer site is very close to an industrial park, where the heavy polluted industries are located, i.e., steel and cement plants. Therefore, the sun photometer measurements are expect to be higher than the MAX-DOAS observations. Accounting for these effects, the MAX-DOAS and sun photometer observation agrees well with each other and the MAX-DOAS derived aerosol profiles are reliable for the retrieval of NO_2 and HCHO profiles.

3.2 Comparison of MAX-DOAS and OMI observations

Vertical column densities of NO_2 and HCHO retrieved from the ground based MAX-DOAS measurements are compared to OMI satellite observations. MAX-DOAS data are temporally averaged around the OMI overpass time from 12:00 to 14:00 (local time), while OMI VCDs are spatially averaged for pixels within 20 km of the MAX-DOAS measurement site. Time series of MAX-DOAS and OMI observations of NO_2 and HCHO VCDs are shown in Figure 2 and Figure 3, respectively. Both OMI NO_2 and HCHO datasets are filtered for cloud radiance fraction smaller than 0.4. Daily and monthly averaged data are shown. Missing data for some months are due to cloud filtering or instrumental issues of the MAX-DOAS.

pNO_2 VCDs measured by the MAX-DOAS and the OMI satellite shows a similar seasonal pattern with higher NO_2 columns during winter and lower NO_2 values over summer. Higher NO_2 levels are due to higher domestic heating emissions and longer atmospheric lifetime of NO_2 during winter. The MAX-DOAS and OMI observations show good temporal consistency with each other with Pearson correlation coefficient (R) of 0.91. Despite the strong correlation between the two datasets, the OMI observations is systematically underestimating the NO_2 columns. The slope and offset of the total least squares regression between the two datasets is 0.50 and -1.89 $\times 10^{15}$ molec/cm^2, respectively. Averaged OMI NO_2 column over Nanjing is 5.67 $\times 10^{15}$ molec/cm^2 which is about a factor 3 lower than the MAX-DOAS averaged VCD of 14.96 $\times 10^{15}$ molec/cm^2

Atmos. Chem. Phys. Discuss., https://doi.org/10.5194/acp-2018-1266
Manuscript under review for journal Atmos. Chem. Phys.
Discussion started: 2 January 2019

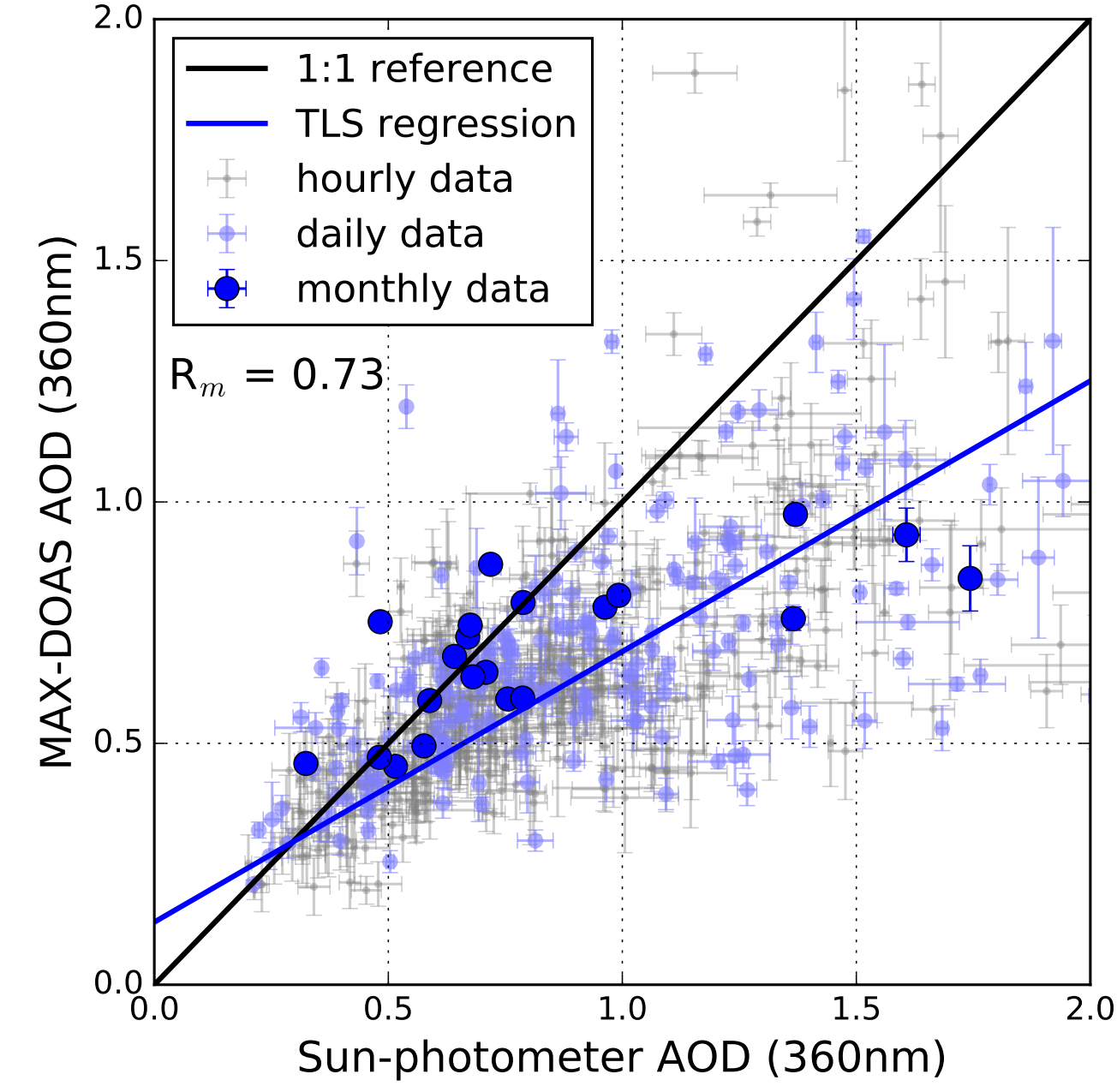

Figure 1. Comparison of AOD measured by the MAX-DOAS and sunphotometer. The total least squares regression line is calculated based on the daily data.

Atmos. Chem. Phys. Discuss., https://doi.org/10.5194/acp-2018-1266
Manuscript under review for journal Atmos. Chem. Phys.
Discussion started: 2 January 2019

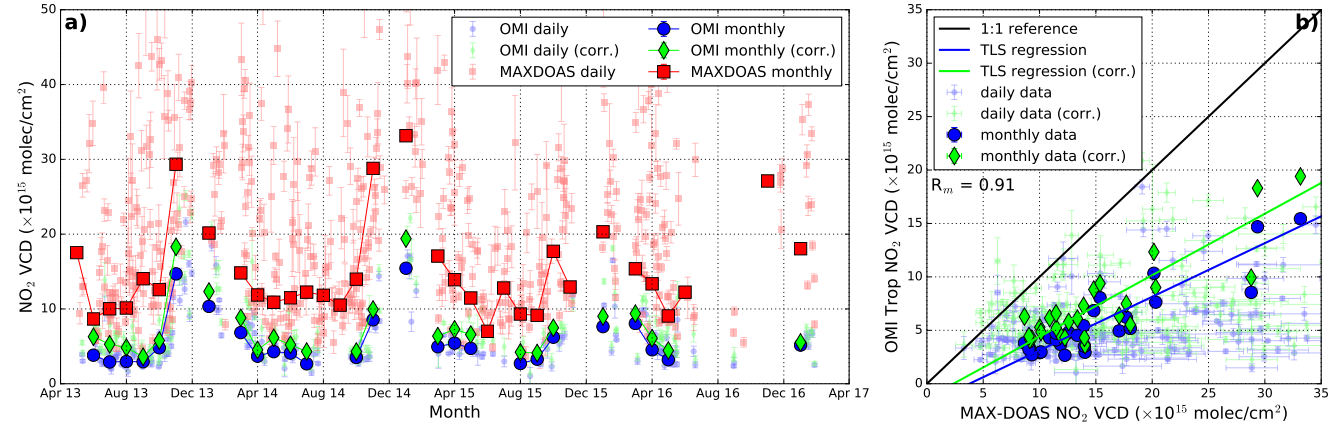

Figure 2. (a) Time series of the MAX-DOAS (red markers) and OMI (blue markers) tropospheric NO_2 VCDs over Nanjing from 2013 to 2017. MAX-DOAS data are temporally averaged around the OMI overpass time. OMI measurements are spatially averaged for pixels within 20 km of the MAX-DOAS measurement site. OMI NO_2 VCDs retrieved using MAX-DOAS profile as a priori information are indicated as green markers. (b) Comparison of tropospheric NO_2 VCDs between the MAX-DOAS and OMI satellite observations. The total least squares regression line is calculated based on the monthly average data.

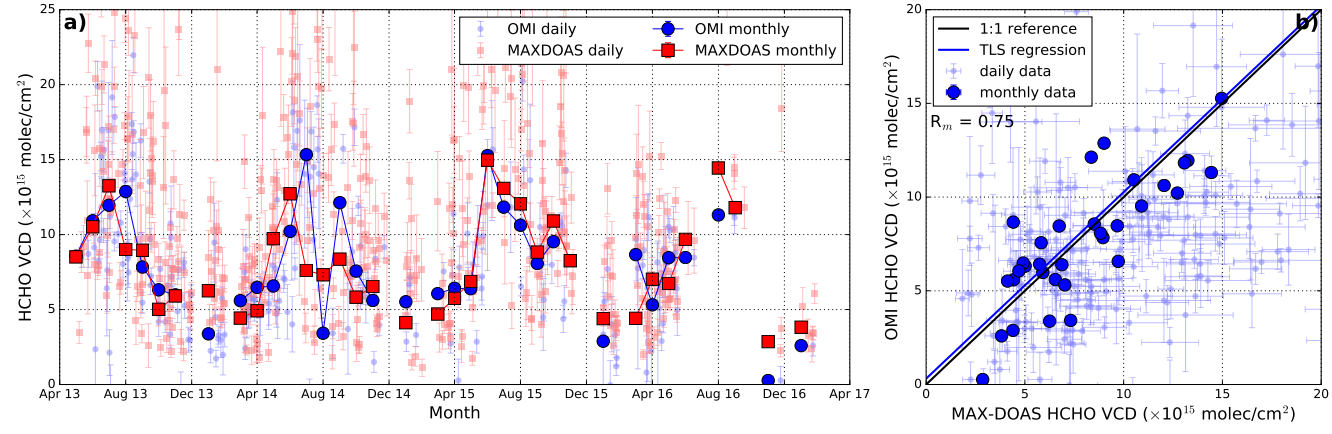

Figure 3. (a) Time series of the MAX-DOAS (red markers) and OMI (blue markers) HCHO VCDs over Nanjing from 2013 to 2017. MAX-DOAS data are temporally averaged around the OMI overpass time. OMI measurements are spatially averaged for pixels within 20 km of the MAX-DOAS measurement site. (b) Comparison of HCHO VCDs between the MAX-DOAS and OMI satellite observations. The total least squares regression line is calculated based on the monthly average data.

(see Figure 2). The underestimation of NO_2 VCDs from OMI measurements agree with previous studies in the Yangtze Delta (Chan et al., 2015; Wang et al., 2017). The discrepancies are mainly related to the differences in spatial coverage between the

ground based and satellite observations and the uncertainties related to the NO_2 vertical distribution profile shape used in the air mass factor calculation. We quantified the influence of NO_2 vertical distribution profile on the air mass factor calculation by recomputed the OMI tropospheric NO_2 air mass factor using the MAX-DOAS NO_2 profile as a priori information. OMI NO_2 VCDs retrieved with MAX-DOAS NO_2 profiles are also indicated in Figure 2. Using the MAX-DOAS profile as a priori information in the OMI NO_2 VCDs retrieval on average increased the OMI NO_2 VCDs by $\sim$30 % with correlation nearly unchanged. The averaged OMI NO_2 column over Nanjing increased to 7.29×10^{15} molec/cm^2. In addition, the slope of the regression line increases from 0.50 to 0.57 while the offset reduces from -1.89 to -1.35 $\times 10^{15}$ molec/cm^2. The result indicates that a better estimation of NO_2 vertical distribution in the satellite VCD retrieval reduces the discrepancies. Our findings agree with previous studies that using better estimated NO_2 vertical profile in the satellite air mass factor calculation enhanced the OMI NO_2 columns and reduced discrepancies between OMI and ground based observations (Chan et al., 2012; Lin et al., 2014; Chan et al., 2015; Wang et al., 2017). However, the improved OMI NO_2 VCDs are still about a factor of 2 lower than the MAX-DOAS observations indicating that there are still remaining issues. The spatial coverage of the OMI measurement footprint is ranging from 330 km^2 up to 4600 km^2 with an average of 920 km^2. Measurements with such large spatial coverage are probably difficult to capture the spatial gradient of NO_2 and resulted in an underestimation over pollution hot spots due to the averaging of large OMI footprint. This effect is especially significant over Nanjing, as it is a local pollution hot spot surrounded by rather clean areas. The underestimation of NO_2 columns is coherent with previous measurements over urban pollution hot spots, i.e., Washington DC and Shanghai (Wenig et al., 2008; Chan et al., 2015). In addition, previous measurements over suburban area in Shanghai show better agreement with OMI observations compared to the measurements in the city (Chan et al., 2015) indicating the effect of spatial inhomogeneity of NO_2 on the satellite data comparison. However, the impact of this effect is difficult to quantify due to lack of high spatial resolution data. Cloud contamination could be an important source of error in the satellite retrieval. Previous study show that the cloud effect on OMI NO_2 VCD retrieval is only significant for cloud radiance fraction > 0.4 (Wang et al., 2017). However, OMI NO_2 data used in this study are filtered for cloud radiance fraction smaller than 0.4. Therefore, cloud contamination should only show a tiny impact in the comparison.

We have also compared the MAX-DOAS and OMI observations of HCHO and both datasets show a similar seasonal variation pattern. The seasonal variation pattern of HCHO is opposite to NO_2 with higher HCHO columns during summer and lower in winter. Higher HCHO levels in summer are mainly related to the increases of biogenic emission of VOCs from plants. The MAX-DOAS measurements of HCHO VCDs agree well with the OMI observations with Pearson correlation coefficient (R) of 0.75. In addition, the absolute value of the columns show a perfect agreement. The average HCHO VCD measured by the MAX-DOAS is 8.04×10^{15} molec/cm^2 while the averaged OMI HCHO VCD is 7.89×10^{15} molec/cm^2. The slope of the total least squares regression between the two datasets is 0.99 with an offset of 0.31×10^{15} molec/cm^2 (see Figure 2b). Slightly lower HCHO VCDs measured by the MAX-DOAS is due the MAX-DOAS measurements are not sensitive to HCHO at higher altitude. Sources of HCHO in the troposphere include the oxidation of varies of VOCs, including methane. Some of these VOCs have relatively long atmospheric lifetime, e.g., methane, therefore, they are rather well mixed in the atmospheric and resulting in a larger portion of HCHO in the upper troposphere. The MAX-DOAS could not capture HCHO at higher altitudes and results in underestimating the HCHO total columns.

Atmos. Chem. Phys. Discuss., https://doi.org/10.5194/acp-2018-1266
Manuscript under review for journal Atmos. Chem. Phys.
Discussion started: 2 January 2019

Atmospheric Chemistry and Physics Discussions

3.3 Seasonal variation of aerosol, NO_2 and HCHO vertical profiles

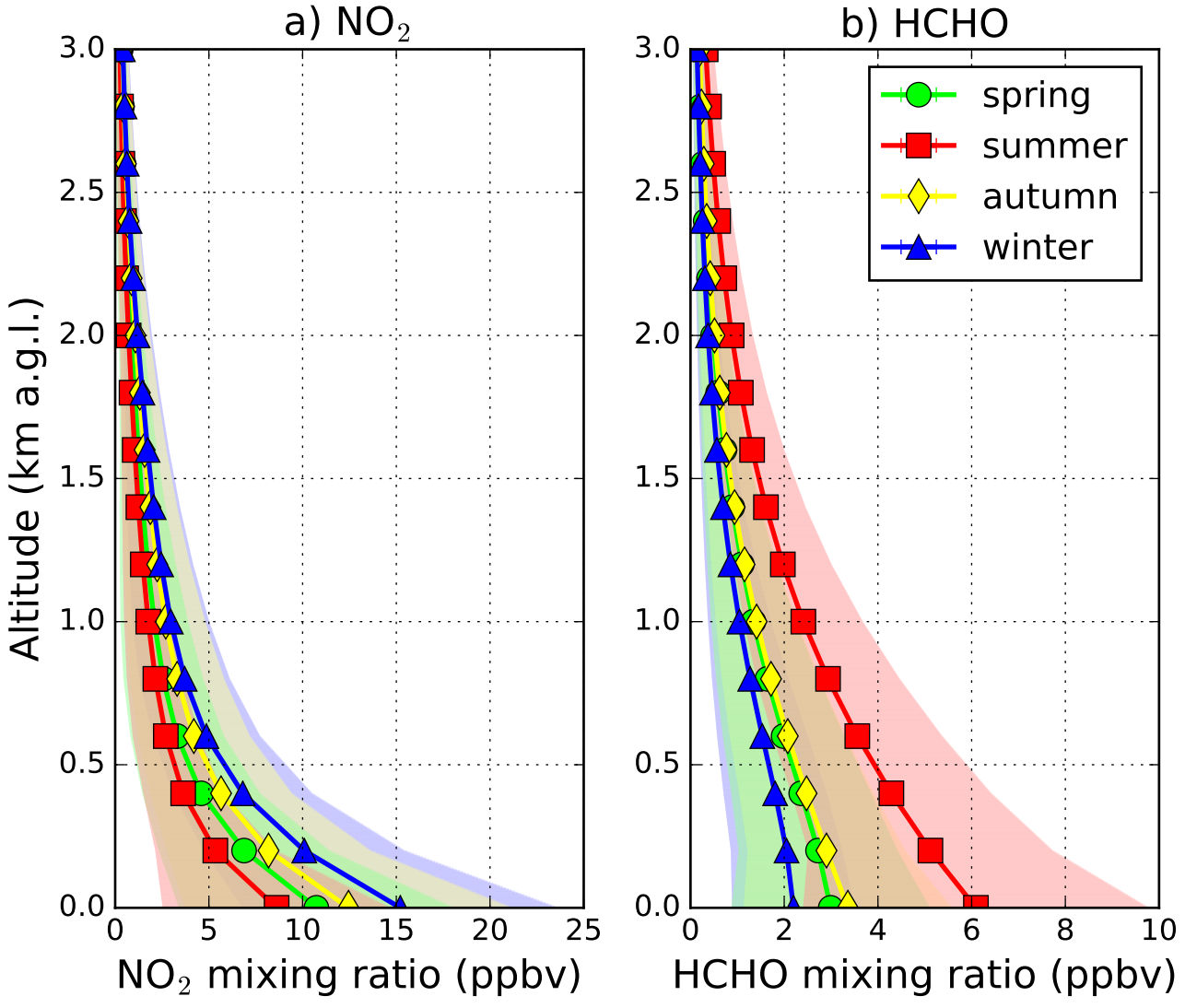

Figure 4. Vertical distribution of (a) aerosol, (b) NO_2 and (c) HCHO for different seasons. Shaded areas represent 1 σ standard deviation of variation.

The seasonal variations of pollutant are closely related to meteorological conditions as well as the characteristics of different emission sources. Analyzing the seasonal variation patterns of different atmospheric pollutants can provide further information on the emission source characteristic as well as the atmospheric processes. Figure 4 shows the vertical profiles of NO_2 and

Atmos. Chem. Phys. Discuss., https://doi.org/10.5194/acp-2018-1266
Manuscript under review for journal Atmos. Chem. Phys.
Discussion started: 2 January 2019

Atmospheric Chemistry and Physics Discussions

HCHO for all four seasons. Significant seasonal patterns are observed from the NO_2 and HCHO data. The NO_2 vertical profiles show higher NO_2 maxing ratios in autumn and winter and lower in spring and summer. NO_2 profiles from all seasons show that the NO_2 mixing ratios decrease with increasing altitude. The result indicates most of the measured NO_2 is produced close to the surface which agrees with the fact that traffic emission is one of the largest source of atmospheric NO_2 in Nanjing. HCHO measurements show a different seasonal variation pattern with lower values during winter and higher mixing ratios in summer. The seasonal pattern of HCHO indicates the significant contribution from biogenic emissions from vegetation. Although HCHO profiles for all seasons also show decreasing mixing ratio with height, the decreasing rate is in general much lower than that of NO_2. Larger fraction of HCHO is located at higher altitudes. This is probably related to the source characteristic of HCHO. Majority of the tropospheric HCHO is secondary produced from the oxidation of VOCs and resulting in a larger portion of HCHO in the upper altitudes.

3.4 Regional pollution transport

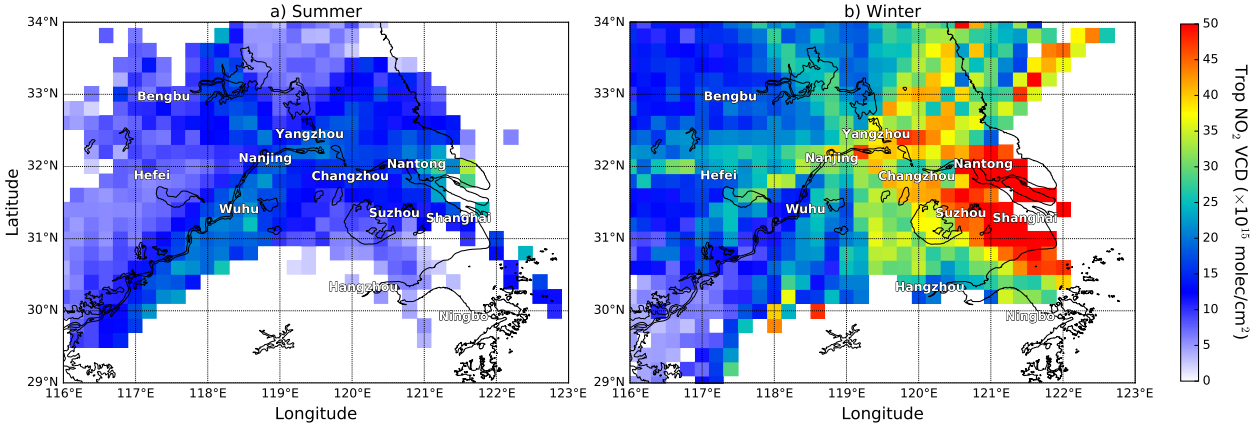

Figure 5. (a) Summer and (b) winter NO_2 fields reconstructed from the MAX-DOAS measurements using backward trajectories calculated by the HYSPLIT model. Backward trajectories are calculated over 6 h for summer measurements and 12 h for winter measurements.

Air pollutants released to the atmosphere do not only cause local impacts, but also can influence regions far from the source through regional transport. In order to investigate the influences from regional transportation of air pollutants, we use the backward trajectories calculated by the HYSPLIT model to back correlate the possible source regions of the MAX-DOAS measured NO_2. Backward trajectories are calculated at the middle point of each MAX-DOAS retrieval layer below 2 km. The MAX-DOAS measurement of NO_2 columns are then assigned to the grid points along the backward trajectories. In this study, the backward propagated NO_2 data are binned in a resolution of $0.25° \times 0.25°$ grid. As NO_2 is a relatively short life pollutants in the atmosphere, it is less likely to travel a long distance from the sources. For this reason, an age weighting factor (w_τ)

Atmos. Chem. Phys. Discuss., https://doi.org/10.5194/acp-2018-1266
Manuscript under review for journal Atmos. Chem. Phys.
Discussion started: 2 January 2019

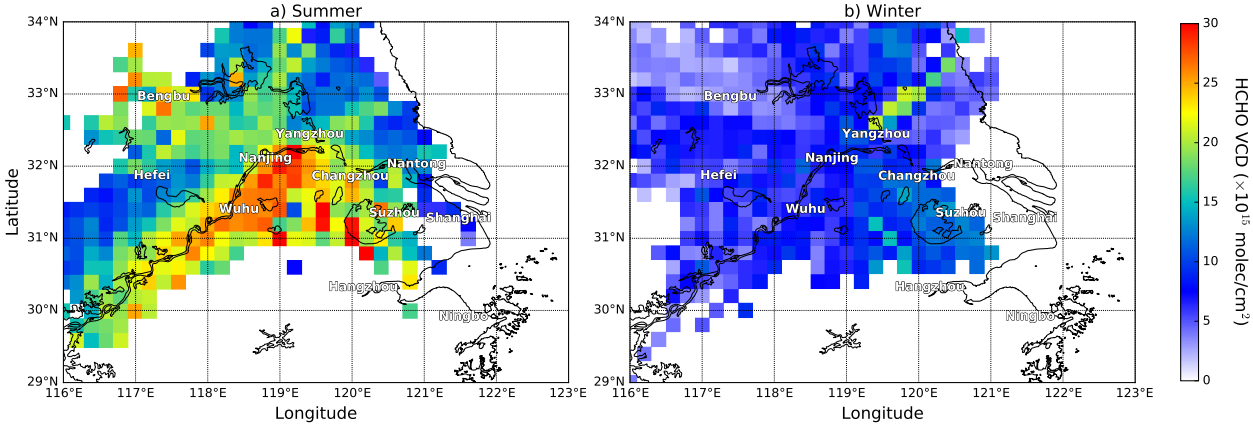

Figure 6. (a) Summer and (b) winter HCHO fields reconstructed from the MAX-DOAS measurements using backward trajectories calculated by the HYSPLIT model. Backward trajectories are calculated over 6 h for summer measurements and 12 h for winter measurements.

is used in the backward propagation. The lifetime weighting factor is defined by Eq. 1 where τ is the lifetime of NO_2 and t represents the time for the air mass to travel to the measurement site.

$$w_\tau = e^{-\frac{t}{\tau}} \tag{1}$$

As the lifetime of NO_2 has a strong seasonal variability, we separate the measurements into summer (June, July and August) and winter (December, January and February) in our analysis. We assume the NO_2 lifetime in summer and winter is 3 h and 6 h, respectively. Backward trajectories are calculated over 6 h for summer measurements and 12 h for winter measurements. NO_2 fields reconstructed from the MAX-DOAS measurements using backward trajectories calculated by the HYSPLIT model are shown in Figure 5. Figure 7 shows the averaged OMI satellite observations of NO_2 and HCHO during summer (June, July and August) and winter (December, January and February) from June 2013 to February 2017. The OMI measurements show that Nanjing has serious NO_2 pollution problem in winter while HCHO being another air pollution problem during summer.

The reconstructed NO_2 fields show a good spatial agreement with OMI satellite observations. However, the reconstructed NO_2 fields are on average 3 times higher than the OMI observations. This agree well with the fact that MAX-DOAS NO_2 VCDs are on average 3 times higher than the OMI data. Elevated NO_2 levels are observed during winter when air mass coming from the east, e.g., Shanghai, Suzhou and Nantong, where OMI observations also show high NO_2 levels. The summer time NO_2 levels are in general lower. However, elevated values can still be observed along the Yangtze River and over some cities, e.g., Nantong and Wuhu. We have also applied the same approach to the MAX-DOAS HCHO measurements with HCHO lifetime of 1 h and 2 h for summer and winter measurements, respectively. HCHO fields reconstructed from the MAX-DOAS measurements are shown in Figure 6. Summer time HCHO data are in general higher than the observations during winter. However, the spatial distribution of the back propagated HCHO data does not show a strong correlation with the

Atmos. Chem. Phys. Discuss., https://doi.org/10.5194/acp-2018-1266
Manuscript under review for journal Atmos. Chem. Phys.
Discussion started: 2 January 2019

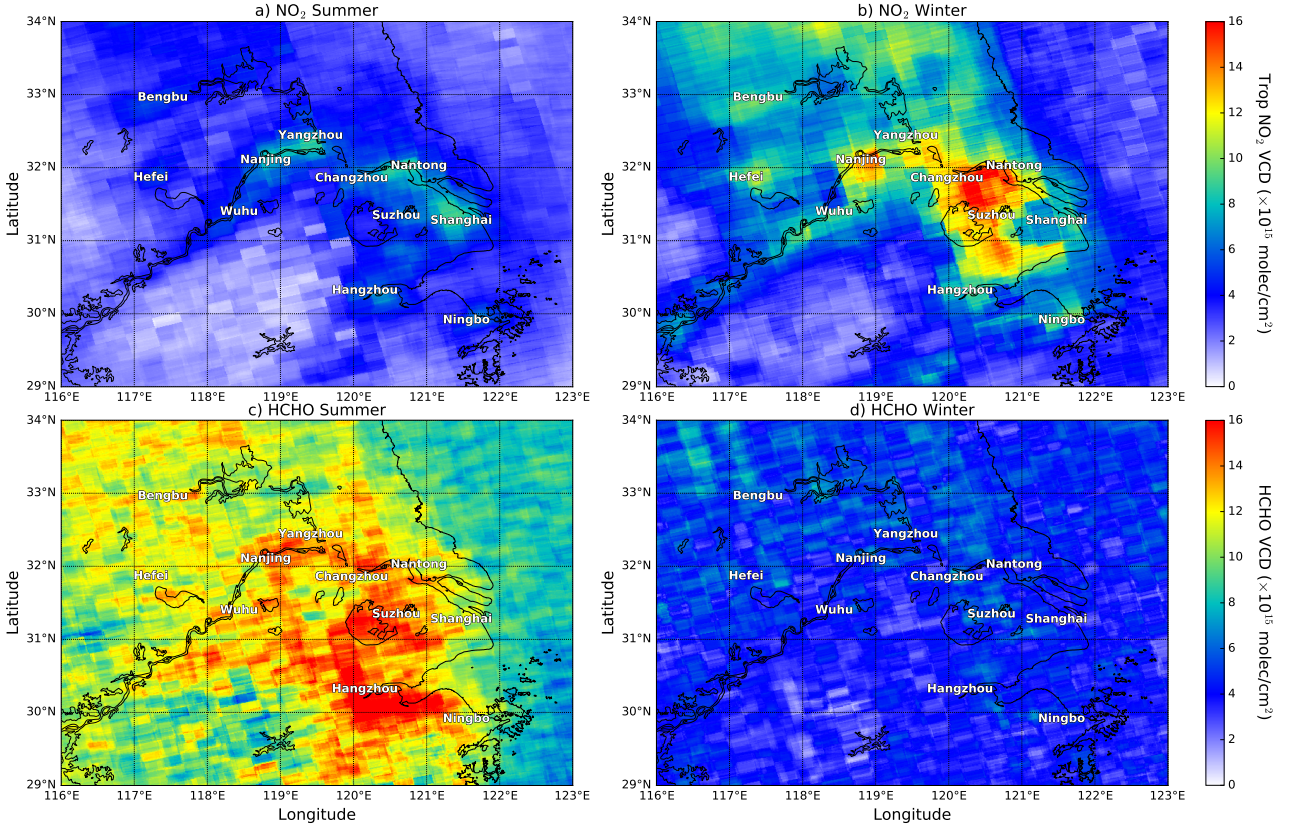

Figure 7. Average OMI NO_2 (top panels) and HCHO (bottom panels) vertical column densities over the Yangtze River delta. OMI observations are averaged from June 2013 to February 2017 and separated into summer time (June, July and August, left panels) and winter time (December, January and February, right panels) measurements. Major cities in the Yangtze River delta are indicated on the map.

OMI satellite observations as the NO_2 data. This is probably due to HCHO is mostly secondary produced in the atmosphere and less related to direct emissions. In addition, the atmospheric lifetime of HCHO is much shorter compared to NO_2 and therefore more dependent on the local productions. The result suggests that the MAX-DOAS measurements are sensitive to the regional transport of air pollutants and implied that the air quality of Nanjing is significantly influenced by the air pollution transportation, especially during winter.

3.5 Assessments of emission reduction during Youth Olympic

The summer Youth Olympic Games was held from 16 to 28 August 2014 in Nanjing, China. During the event, the government implemented a series of air pollution control measures. Heavy emission vehicles were strictly prohibited. Local heavy industries, e.g., petrochemical and steel industries were required to limit their production during the Youth Olympic Games.

Atmos. Chem. Phys. Discuss., https://doi.org/10.5194/acp-2018-1266
Manuscript under review for journal Atmos. Chem. Phys.
Discussion started: 2 January 2019

Atmospheric Chemistry and Physics Discussions

These air pollution control measures were often implemented when such an international events held in China (Wu et al., 2013; Wang et al., 2014; Chan et al., 2015; Liu et al., 2016; Sun et al., 2016). In order to study the influences of the emission control measures implemented during the Youth Olympic Games on the local air quality, we compare the MAX-DOAS observations of aerosol, NO_2 and HCHO taken before, during and after the Youth Olympic Games. We define the pre-Olympic period from a month before the Youth Olympic Games (16 July 2014) to 1 day before the Youth Olympic Games (15 August 2014). During the pre-Olympic period, the government gradually started to implement some of the emission control measures. During the Youth Olympic Games all those air pollution control measures were strictly implemented. The post-Olympic period is defined from 29 August 2014 to 28 September 2014 where the emission control was gradually getting back to normal.

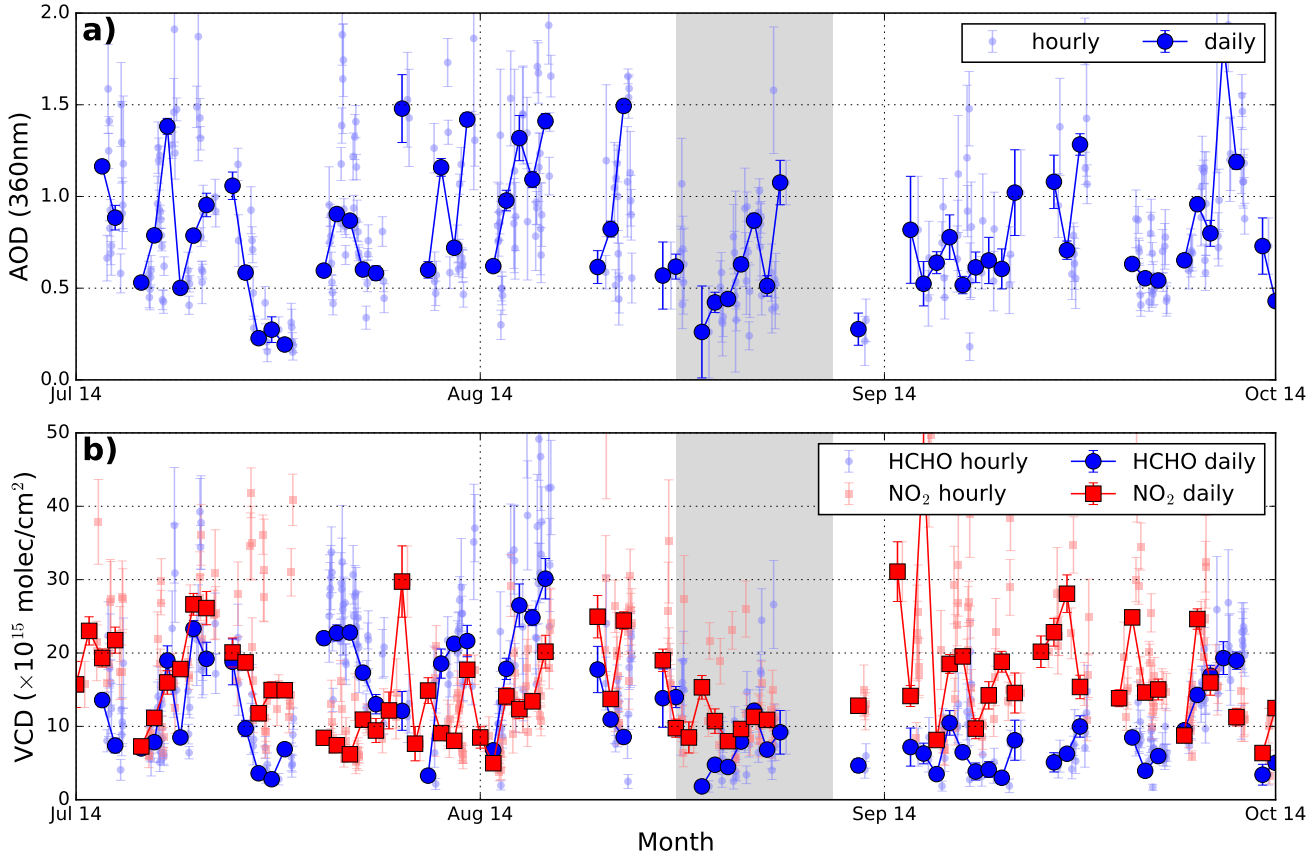

Figure 8. Time series of (a) aerosol optical depths, (b) HCHO and NO_2 VCDs measured by the MAX-DOAS around the Youth Olympic Games. Hourly and daily averaged values are shown. The gray shadowed area indicates the Youth Olympic Games period (16 to 28 August 2014).

Atmos. Chem. Phys. Discuss., https://doi.org/10.5194/acp-2018-1266
Manuscript under review for journal Atmos. Chem. Phys.
Discussion started: 2 January 2019

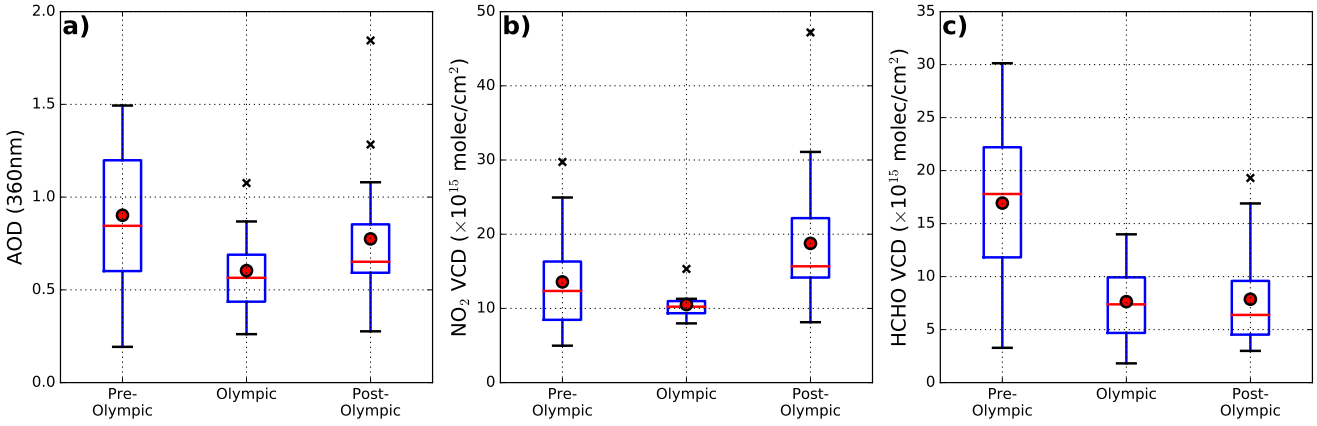

Figure 9. Boxplots of (a) aerosol optical depths, (b) NO_2 and (c) HCHO VCDs before, during and after the Youth Olympic Games.

Time series of aerosol optical depths, HCHO and NO_2 VCDs measured by the MAX-DOAS around the Youth Olympic Games are shown in Figure 8. The gray shadowed area indicates the Youth Olympic Games period (16 to 28 August 2014). The AODs, HCHO and NO_2 measurements show a strong temporal variability. In order to investigate the effect of the Youth Olympic Games, we analyzed the statistic of AODs, HCHO and NO_2 VCDs for the pre-Olympic, Olympic and post-Olympic periods. Boxplots of the AODs, HCHO and NO_2 VCDs for the three periods are shown in Figure 9. The results show that AOD, NO_2 and HCHO VCD are the lowest during the Olympic period among those 3 periods. The MAX-DOAS measurements of AOD reduced from 0.9 during the pre-Olympic period to 0.6 for the Olympic period and bounced back to about 0.8 after the Youth Olympic Games. A reduction of NO_2 columns can also be observed during the Youth Olympic Games. Averaged NO_2 VCDs are 14, 11 and 19×10^{15} molec/cm^2 for periods before, during and after the Youth Olympic Games, respectively. The HCHO columns measured during the Youth Olympic Games also decreased by more than $\sim$50 % from 17×10^{15} molec/cm^2 before the Olympic down to 8×10^{15} molec/cm^2 during the Youth Olympic Games. As the meteorological conditions are very similar during the three periods, the decrease of pollutant concentrations are mainly attributed to the reduction of emissions during the Youth Olympic Games.

4 Summary and conclusions

In this paper, we present long term observations of atmospheric NO_2 and HCHO in Nanjing using a MAX-DOAS instrument. Ground based MAX-DOAS measurements were performed from April 2013 to February 2017. Differential slant columns of O_4, NO_2 and HCHO were retrieved by applying the differential optical absorption technique to the scattered sun light spectra at the UV band. The results are served as inputs for the retrieval of aerosol extinction, NO_2 and HCHO profiles in the lower troposphere.

Aerosol results derived from the MAX-DOAS observations are validated by comparing the AODs to sun photometer observations. The MAX-DOAS and sun photometer measurements show a good agreement with each other with Pearson correlation coefficient (R) of 0.73. Considering the differences in measurement technique and measurement location, we concluded that the MAX-DOAS aerosol measurements are reliable for the NO_2 and HCHO profile retrieval.

Tropospheric vertical column densities (VCDs) of NO_2 derived from MAX-DOAS measurements are used to validate OMI observations. The comparison shows that the OMI observations correlate well with the MAX-DOAS data with Pearson correlation coefficient (R) of 0.91. However, OMI observations are on average a factor of 3 lower than the MAX-DOAS measurements. Using the MAX-DOAS NO_2 profile as a priori information in the OMI retrieval on average increased the OMI NO_2 VCDs by $\sim$30 % with correlation nearly unchanged. However, the improved OMI NO_2 VCDs are still about a factor of 2 lower than the MAX-DOAS observations. The remaining discrepancy is mainly related to the difference in spatial coverage between the two measurements. We also compared the OMI observation of HCHO VCDs to our MAX-DOAS data. The result shows a good agreement between the two datasets with R of 0.75 and the slope of the regression line is 0.99.

The MAX-DOAS measurement of NO_2 and HCHO profiles are analyzed together with the backward trajectory simulations to assess the regional transportation and possible source regions of the MAX-DOAS measured NO_2 and HCHO. The age weighted backward propagation approach is used to reconstruct the spatial distribution of NO_2 and HCHO over the Yangtze River Delta during summer and winter time. The reconstructed NO_2 fields show a distinct agreement with OMI satellite observations. The result shows the MAX-DOAS measurements are sensitive to the air pollution transportation in the Yangtze River Delta. However, due to the short atmospheric lifetime of HCHO, the backward propagated HCHO data does not show a strong spatial correlation with the OMI HCHO observations. Our result suggested the air quality of Nanjing are significantly influenced by air pollution transportation, especially during winter.

We have also used the MAX-DOAS observations of aerosol, NO_2 and HCHO for the investigation of the effectiveness of air pollution control measures implemented during the Youth Olympic Games 2014. Our results show a significant reduction (30 % - 50 %) of ambient aerosol, NO_2 and HCHO compared to measurements before and after the Youth Olympic games. The results indicate the effects of the reduction of emissions during the Youth Olympic Games. Our findings provide a better understanding of the transportation and sources of pollutants in the Yangtze River Delta as well as the effects of emission control measures during large international event, which are important for the future design of air pollution control policies.

Author contributions. KLC, AD, KPH and NH designed the experiment. KLC, ZW, AD, YS and NH carried out the experiment. JW and FZ provided auxiliary data. MW provided useful comments for the discussion. KLC analyzed the measurement data and prepared the manuscript with contributions from all co-authors.

Competing interests. The authors declare that they have no conflict of interest.

Atmos. Chem. Phys. Discuss., https://doi.org/10.5194/acp-2018-1266
Manuscript under review for journal Atmos. Chem. Phys.
Discussion started: 2 January 2019

Acknowledgements. The authors would also like to thank the National Oceanic and Atmospheric Administration (NOAA) Air Resources Laboratory (ARL) for the provision of the HYSPLIT transport and dispersion model used in this publication. The work described in this paper was partly supported by the ESA-MOST Dragon 3 Cooperation Programme under the framework of the East Asian monsoon and air quality project.

References

Aliwell, S. R., Roozendael, M. V., Johnston, P. V., Richter, A., Wagner, T., Arlander, D. W., Burrows, J. P., Fish, D. J., Jones, R. L., Tørnkvist, K. K., Lambert, J.-C., Pfeilsticker, K., and Pundt, I.: Analysis for BrO in zenith-sky spectra: An intercomparison exercise for analysis improvement, Journal of Geophysical Research: Atmospheres, 107, ACH 10–1–ACH 10–20, https://doi.org/10.1029/2001JD000329, 2002.

Ångström, A.: On the Atmospheric Transmission of Sun Radiation and on Dust in the Air, Geografiska Annaler, 11, 156–166, https://doi.org/10.1080/20014422.1929.11880498, 1929.

Beirle, S., Platt, U., Wenig, M., and Wagner, T.: Weekly cycle of NO_2 by GOME measurements: a signature of anthropogenic sources, Atmospheric Chemistry and Physics, 3, 2225–2232, https://doi.org/10.5194/acp-3-2225-2003, 2003.

Beirle, S., Platt, U., Wenig, M., and Wagner, T.: NO_x production by lightning estimated with GOME, Advances in Space Research, 34, 793–797, https://doi.org/http://dx.doi.org/10.1016/j.asr.2003.07.069, 2004.

Bond, D. W., Zhang, R., Tie, X., Brasseur, G., Huffines, G., Orville, R. E., and Boccippio, D. J.: NO_x production by lightning over the continental United States, Journal of Geophysical Research: Atmospheres, 106, 27 701–27 710, https://doi.org/10.1029/2000JD000191, http://dx.doi.org/10.1029/2000JD000191, 2001.

Bovensmann, H., Burrows, J., Buchwitz, M., Frerick, J., Noël, S., Rozanov, V., Chance, K., and Goede, A.: SCIAMACHY: Mission objectives and measurement modes, Journal of the Atmospheric Sciences, 56, 127–150, 1999.

Bucsela, E. J., Krotkov, N. A., Celarier, E. A., Lamsal, L. N., Swartz, W. H., Bhartia, P. K., Boersma, K. F., Veefkind, J. P., Gleason, J. F., and Pickering, K. E.: A new stratospheric and tropospheric NO_2 retrieval algorithm for nadir-viewing satellite instruments: applications to OMI, Atmospheric Measurement Techniques, 6, 2607–2626, https://doi.org/10.5194/amt-6-2607-2013, 2013.

Burrows, J. P., Weber, M., Buchwitz, M., Rozanov, V., Ladstätter-Weißenmayer, A., Richter, A., DeBeek, R., Hoogen, R., Bramstedt, K., Eichmann, K.-U., et al.: The global ozone monitoring experiment (GOME): Mission concept and first scientific results, Journal of the Atmospheric Sciences, 56, 151–175, 1999.

Callies, J., Corpaccioli, E., Eisinger, M., Hahne, A., and Lefebvre, A.: GOME-2-Metop's second-generation sensor for operational ozone monitoring, ESA bulletin, 102, 28–36, 2000.

Chan, K. L., Pöhler, D., Kuhlmann, G., Hartl, A., Platt, U., and Wenig, M. O.: NO_2 measurements in Hong Kong using LED based long path differential optical absorption spectroscopy, Atmospheric Measurement Techniques, 5, 901–912, https://doi.org/10.5194/amt-5-901-2012, 2012.

Chan, K. L., Hartl, A., Lam, Y. F., Xie, P. H., Liu, W. Q., Cheung, H. M., Lampel, J., Pöhler, D., Li, A., Xu, J., Zhou, H. J., Ning, Z., and Wenig, M.: Observations of tropospheric NO_2 using ground based MAX-DOAS and OMI measurements during the Shanghai World Expo 2010, Atmospheric Environment, 119, 45–58, https://doi.org/http://dx.doi.org/10.1016/j.atmosenv.2015.08.041, 2015.

Chan, K. L., Wiegner, M., Wenig, M., and Pöhler, D.: Observations of tropospheric aerosols and NO_2 in Hong Kong over 5 years using ground based MAX-DOAS, Science of The Total Environment, 619-620, 1545 – 1556, https://doi.org/https://doi.org/10.1016/j.scitotenv.2017.10.153, 2018.

Clémer, K., Van Roozendael, M., Fayt, C., Hendrick, F., Hermans, C., Pinardi, G., Spurr, R., Wang, P., and De Mazière, M.: Multiple wavelength retrieval of tropospheric aerosol optical properties from MAXDOAS measurements in Beijing, Atmospheric Measurement Techniques, 3, 863–878, https://doi.org/10.5194/amt-3-863-2010, 2010.

Cleveland, W. S.: LOWESS: A Program for Smoothing Scatterplots by Robust Locally Weighted Regression, The American Statistician, 35, https://doi.org/10.2307/2683591, 1981.

Crutzen, P. J.: The influence of nitrogen oxides on the atmospheric ozone content, Quarterly Journal of the Royal Meteorological Society, 96, 320–325, https://doi.org/10.1002/qj.49709640815, 1970.

De Smedt, I., Theys, N., Yu, H., Danckaert, T., Lerot, C., Compernolle, S., Van Roozendael, M., Richter, A., Hilboll, A., Peters, E., Pedergnana, M., Loyola, D., Beirle, S., Wagner, T., Eskes, H., van Geffen, J., Boersma, K. F., and Veefkind, P.: Algorithm theoretical baseline for formaldehyde retrievals from S5P TROPOMI and from the QA4ECV project, Atmospheric Measurement Techniques, 11, 2395–2426, https://doi.org/10.5194/amt-11-2395-2018, 2018.

Emde, C., Buras-Schnell, R., Kylling, A., Mayer, B., Gasteiger, J., Hamann, U., Kylling, J., Richter, B., Pause, C., Dowling, T., and Bugliaro, L.: The libRadtran software package for radiative transfer calculations (version 2.0.1), Geoscientific Model Development, 9, 1647–1672, https://doi.org/10.5194/gmd-9-1647-2016, 2016.

Fleischmann, O. C., Burrows, J. P., and Orphal, J.: Time-windowing Fourier transform absorption spectroscopy for flash photolysis investigations, Journal of Photochemistry and Photobiology A: Chemistry, 157, 127–136, https://doi.org/http://dx.doi.org/10.1016/S1010-6030(03)00069-8, atmospheric Photochemistry, 2003.

Fried, A., Cantrell, C., Olson, J., Crawford, J. H., Weibring, P., Walega, J., Richter, D., Junkermann, W., Volkamer, R., Sinreich, R., Heikes, B. G., O'Sullivan, D., Blake, D. R., Blake, N., Meinardi, S., Apel, E., Weinheimer, A., Knapp, D., Perring, A., Cohen, R. C., Fuelberg, H., Shetter, R. E., Hall, S. R., Ullmann, K., Brune, W. H., Mao, J., Ren, X., Huey, L. G., Singh, H. B., Hair, J. W., Riemer, D., Diskin, G., and Sachse, G.: Detailed comparisons of airborne formaldehyde measurements with box models during the 2006 INTEX-B and MILAGRO campaigns: potential evidence for significant impacts of unmeasured and multi-generation volatile organic carbon compounds, Atmospheric Chemistry and Physics, 11, 11 867–11 894, https://doi.org/10.5194/acp-11-11867-2011, 2011.

Frieß, U., Monks, P. S., Remedios, J. J., Rozanov, A., Sinreich, R., Wagner, T., and Platt, U.: MAX-DOAS O_4 measurements: A new technique to derive information on atmospheric aerosols: 2. Modeling studies, Journal of Geophysical Research: Atmospheres, 111, https://doi.org/10.1029/2005JD006618, 2006.

González Abad, G., Liu, X., Chance, K., Wang, H., Kurosu, T. P., and Suleiman, R.: Updated Smithsonian Astrophysical Observatory Ozone Monitoring Instrument (SAO OMI) formaldehyde retrieval, Atmospheric Measurement Techniques, 8, 19–32, https://doi.org/10.5194/amt-8-19-2015, 2015.

Halla, J. D., Wagner, T., Beirle, S., Brook, J. R., Hayden, K. L., O'Brien, J. M., Ng, A., Majonis, D., Wenig, M. O., and McLaren, R.: Determination of tropospheric vertical columns of NO_2 and aerosol optical properties in a rural setting using MAX-DOAS, Atmospheric Chemistry and Physics, 11, 12 475–12 498, https://doi.org/10.5194/acp-11-12475-2011, 2011.

Hartl, A. and Wenig, M. O.: Regularisation model study for the least-squares retrieval of aerosol extinction time series from UV/VIS MAX-DOAS observations for a ground layer profile parameterisation, Atmospheric Measurement Techniques, 6, 1959–1980, https://doi.org/10.5194/amt-6-1959-2013, 2013.

Hönninger, G. and Platt, U.: Observations of BrO and its vertical distribution during surface ozone depletion at Alert, Atmospheric Environment, 36, 2481–2489, https://doi.org/http://dx.doi.org/10.1016/S1352-2310(02)00104-8, 2002.

Hönninger, G., von Friedeburg, C., and Platt, U.: Multi axis differential optical absorption spectroscopy (MAX-DOAS), Atmospheric Chemistry and Physics, 4, 231–254, https://doi.org/10.5194/acp-4-231-2004, 2004.

Irie, H., Kanaya, Y., Akimoto, H., Iwabuchi, H., Shimizu, A., and Aoki, K.: First retrieval of tropospheric aerosol profiles using MAX-DOAS and comparison with lidar and sky radiometer measurements, Atmospheric Chemistry and Physics, 8, 341–350, https://doi.org/10.5194/acp-8-341-2008, 2008.

Jang, M. and Kamens, R. M.: Characterization of Secondary Aerosol from the Photooxidation of Toluene in the Presence of NO_x and 1-Propene, Environmental Science & Technology, 35, 3626–3639, https://doi.org/10.1021/es010676+, 2001.

Jin, J., Ma, J., Lin, W., Zhao, H., Shaiganfar, R., Beirle, S., and Wagner, T.: MAX-DOAS measurements and satellite validation of tropospheric NO_2 and SO_2 vertical column densities at a rural site of North China, Atmospheric Environment, 133, 12–25, https://doi.org/http://dx.doi.org/10.1016/j.atmosenv.2016.03.031, 2016.

Krotkov, N. A., Lamsal, L. N., Celarier, E. A., Swartz, W. H., Marchenko, S. V., Bucsela, E. J., Chan, K. L., Wenig, M., and Zara, M.: The version 3 OMI NO_2 standard product, Atmospheric Measurement Techniques, 10, 3133–3149, https://doi.org/10.5194/amt-10-3133-2017, 2017.

Levelt, P., Van den Oord, G. H. J., Dobber, M., Malkki, A., Visser, H., de Vries, J., Stammes, P., Lundell, J., and Saari, H.: The ozone monitoring instrument, Geoscience and Remote Sensing, IEEE Transactions on, 44, 1093–1101, https://doi.org/10.1109/TGRS.2006.872333, 2006.

Li, X., Brauers, T., Shao, M., Garland, R. M., Wagner, T., Deutschmann, T., and Wahner, A.: MAX-DOAS measurements in southern China: retrieval of aerosol extinctions and validation using ground-based in-situ data, Atmospheric Chemistry and Physics, 10, 2079–2089, https://doi.org/10.5194/acp-10-2079-2010, 2010.

Li, X., Brauers, T., Hofzumahaus, A., Lu, K., Li, Y. P., Shao, M., Wagner, T., and Wahner, A.: MAX-DOAS measurements of NO_2, HCHO and CHOCHO at a rural site in Southern China, Atmospheric Chemistry and Physics, 13, 2133–2151, https://doi.org/10.5194/acp-13-2133-2013, 2013.

Lin, J.-T., Martin, R. V., Boersma, K. F., Sneep, M., Stammes, P., Spurr, R., Wang, P., Van Roozendael, M., Clémer, K., and Irie, H.: Retrieving tropospheric nitrogen dioxide from the Ozone Monitoring Instrument: effects of aerosols, surface reflectance anisotropy, and vertical profile of nitrogen dioxide, Atmospheric Chemistry and Physics, 14, 1441–1461, https://doi.org/10.5194/acp-14-1441-2014, 2014.

Liu, H., Liu, C., Xie, Z., Li, Y., Huang, X., Wang, S., Xu, J., and Xie, P.: A paradox for air pollution controlling in China revealed by "APEC Blue" and "Parade Blue", Scientific Reports, 6, 34 408, 2016.

Ma, J. Z., Beirle, S., Jin, J. L., Shaiganfar, R., Yan, P., and Wagner, T.: Tropospheric NO_2 vertical column densities over Beijing: results of the first three years of ground-based MAX-DOAS measurements (2008-2011) and satellite validation, Atmospheric Chemistry and Physics, 13, 1547–1567, https://doi.org/10.5194/acp-13-1547-2013, 2013.

Marchenko, S., Krotkov, N. A., Lamsal, L. N., Celarier, E. A., Swartz, W. H., and Bucsela, E. J.: Revising the slant column density retrieval of nitrogen dioxide observed by the Ozone Monitoring Instrument, Journal of Geophysical Research: Atmospheres, 120, 5670–5692, https://doi.org/10.1002/2014JD022913, http://dx.doi.org/10.1002/2014JD022913, 2014JD022913, 2015.

Meller, R. and Moortgat, G. K.: Temperature dependence of the absorption cross sections of formaldehyde between 223 and 323 K in the wavelength range 225-375 nm, Journal of Geophysical Research: Atmospheres, 105, 7089–7101, https://doi.org/10.1029/1999JD901074, 2000.

Mijling, B., van der A, R. J., Boersma, K. F., Van Roozendael, M., De Smedt, I., and Kelder, H. M.: Reductions of NO_2 detected from space during the 2008 Beijing Olympic Games, Geophysical Research Letters, 36, https://doi.org/10.1029/2009GL038943, 2009.

Ortega, I., Berg, L. K., Ferrare, R. A., Hair, J. W., Hostetler, C. A., and Volkamer, R.: Elevated aerosol layers modify the O_2-O_2 absorption measured by ground-based MAX-DOAS, Journal of Quantitative Spectroscopy and Radiative Transfer, 176, 34–49, https://doi.org/https://doi.org/10.1016/j.jqsrt.2016.02.021, 2016.

Platt, U. and Stutz, J.: Differential optical absorption spectroscopy - principles and applications, Springer, 2008.

Richter, A., Burrows, J. P., Nüß, H., Granier, C., and Niemeier, U.: Increase in tropospheric nitrogen dioxide over China observed from space, Nature, 437, 129–132, 2005.

Rodgers, C. D.: Inverse methods for atmospheric sounding: Theory and practice, vol. 2, World scientific, 2000.

Rotman, D. A., Tannahill, J. R., Kinnison, D. E., Connell, P. S., Bergmann, D., Proctor, D., Rodriguez, J. M., Lin, S. J., Rood, R. B., Prather, M. J., Rasch, P. J., Considine, D. B., Ramaroson, R., and Kawa, S. R.: Global Modeling Initiative assessment model: Model description, integration, and testing of the transport shell, Journal of Geophysical Research: Atmospheres, 106, 1669–1691, https://doi.org/10.1029/2000JD900463, 2001.

Serdyuchenko, A., Gorshelev, V., Weber, M., Chehade, W., and Burrows, J. P.: High spectral resolution ozone absorption cross-sections - Part 2: Temperature dependence, Atmospheric Measurement Techniques, 7, 625–636, https://doi.org/10.5194/amt-7-625-2014, 2014.

Sinreich, R., Frieß, U., Wagner, T., and Platt, U.: Multi axis differential optical absorption spectroscopy (MAX-DOAS) of gas and aerosol distributions, Faraday Discussions, 130, 153, https://doi.org/10.1039/b419274p, 2005.

Solomon, S., Schmeltekopf, A. L., and Sanders, R. W.: On the interpretation of zenith sky absorption measurements, Journal of Geophysical Research: Atmospheres, 92, 8311–8319, https://doi.org/10.1029/JD092iD07p08311, 1987.

Stein, A. F., Draxler, R. R., Rolph, G. D., Stunder, B. J. B., Cohen, M. D., and Ngan, F.: NOAA's HYSPLIT Atmospheric Transport and Dispersion Modeling System, Bulletin of the American Meteorological Society, 96, 2059–2077, https://doi.org/10.1175/BAMS-D-14-00110.1, 2015.

Sun, Y., Wang, Z., Wild, O., Xu, W., Chen, C., Fu, P., Du, W., Zhou, L., Zhang, Q., Han, T., Wang, Q., Pan, X., Zheng, H., Li, J., Guo, X., Liu, J., and Worsnop, D. R.: "APEC Blue": Secondary Aerosol Reductions from Emission Controls in Beijing, Scientific Reports, 6, 20 668, 2016.

Thalman, R. and Volkamer, R.: Temperature dependent absorption cross-sections of O_2-O_2 collision pairs between 340 and 630 nm and at atmospherically relevant pressure, Phys. Chem. Chem. Phys., 15, 15 371–15 381, https://doi.org/10.1039/C3CP50968K, 2013.

van der A, R. J., Eskes, H. J., Boersma, K. F., van Noije, T. P. C., Van Roozendael, M., De Smedt, I., Peters, D. H. M. U., and Meijer, E. W.: Trends, seasonal variability and dominant NO_x source derived from a ten year record of NO_2 measured from space, Journal of Geophysical Research: Atmospheres, 113, https://doi.org/10.1029/2007JD009021, 2008.

Vandaele, A., Hermans, C., Simon, P., Carleer, M., Colin, R., Fally, S., Merienne, M., Jenouvrier, A., and Coquart, B.: Measurements of the NO_2 absorption cross-section from 42000 cm^{-1} to 10000 cm^{-1} (238-1000 nm) at 220 K and 294 K, Journal of Quantitative Spectroscopy and Radiative Transfer, 59, 171 – 184, https://doi.org/http://dx.doi.org/10.1016/S0022-4073(97)00168-4, atmospheric Spectroscopy Applications 96, 1998.

Wagner, T., Dix, B., Friedeburg, C. v., Fries, U., Sanghavi, S., Sinreich, R., and Platt, U.: MAX-DOAS O_4 measurements: A new technique to derive information on atmospheric aerosols - Principles and information content, Journal of Geophysical Research: Atmospheres, 109, https://doi.org/10.1029/2004JD004904, 2004.

Wagner, T., Deutschmann, T., and Platt, U.: Determination of aerosol properties from MAX-DOAS observations of the Ring effect, Atmospheric Measurement Techniques, 2, 495–512, https://doi.org/10.5194/amt-2-495-2009, 2009.

Wagner, T., Beirle, S., Brauers, T., Deutschmann, T., Frieß, U., Hak, C., Halla, J. D., Heue, K. P., Junkermann, W., Li, X., Platt, U., and Pundt-Gruber, I.: Inversion of tropospheric profiles of aerosol extinction and HCHO and NO_2 mixing ratios from MAX-DOAS observations in Milano during the summer of 2003 and comparison with independent data sets, Atmospheric Measurement Techniques, 4, 2685–2715, https://doi.org/10.5194/amt-4-2685-2011, 2011.

Wagner, T., Beirle, S., Benavent, N., Bösch, T., Chan, K. L., Donner, S., Dörner, S., Fayt, C., Frieß, U., García-Nieto, D., Gielen, C., González-Bartolome, D., Gomez, L., Hendrick, F., Henzing, B., Jin, J. L., Lampel, J., Ma, J., Mies, K., Navarro, M., Peters, E., Pinardi, G., Puentedura, O., Puķīte, J., Remmers, J., Richter, A., Saiz-Lopez, A., Shaiganfar, R., Sihler, H., Van Roozendael, M., Wang, Y., and Yela, M.: Is a scaling factor required to obtain closure between measured and modelled atmospheric O_4 absorptions? - A case study for two days during the MADCAT campaign, Atmospheric Measurement Techniques Discussions, 2018, 1–85, https://doi.org/10.5194/amt-2018-238, 2018.

Wang, S., Gao, J., Zhang, Y., Zhang, J., Cha, F., Wang, T., Ren, C., and Wang, W.: Impact of emission control on regional air quality: An observational study of air pollutants before, during and after the Beijing Olympic Games, Journal of Environmental Sciences, 26, 175 – 180, https://doi.org/https://doi.org/10.1016/S1001-0742(13)60395-2, 2014.

Wang, S., Cuevas, C. A., Frieß, U., and Saiz-Lopez, A.: MAX-DOAS retrieval of aerosol extinction properties in Madrid, Spain, Atmospheric Measurement Techniques, 9, 5089–5101, https://doi.org/10.5194/amt-9-5089-2016, 2016.

Wang, Y., Beirle, S., Lampel, J., Koukouli, M., De Smedt, I., Theys, N., Li, A., Wu, D., Xie, P., Liu, C., Van Roozendael, M., Stavrakou, T., Müller, J.-F., and Wagner, T.: Validation of OMI, GOME-2A and GOME-2B tropospheric NO_2, SO_2 and HCHO products using MAX-DOAS observations from 2011 to 2014 in Wuxi, China: investigation of the effects of priori profiles and aerosols on the satellite products, Atmospheric Chemistry and Physics, 17, 5007–5033, https://doi.org/10.5194/acp-17-5007-2017, 2017.

Wenig, M., Spichtinger, N., Stohl, A., Held, G., Beirle, S., Wagner, T., Jähne, B., and Platt, U.: Intercontinental transport of nitrogen oxide pollution plumes, Atmospheric Chemistry and Physics, 3, 387–393, https://doi.org/10.5194/acp-3-387-2003, 2003.

Wenig, M. O., Cede, A. M., Bucsela, E. J., Celarier, E. A., Boersma, K. F., Veefkind, J. P., Brinksma, E. J., Gleason, J. F., and Herman, J. R.: Validation of OMI tropospheric NO_2 column densities using direct-Sun mode Brewer measurements at NASA Goddard Space Flight Center, Journal of Geophysical Research: Atmospheres, 113, https://doi.org/10.1029/2007JD008988, 2008.

Witte, J. C., Schoeberl, M. R., Douglass, A. R., Gleason, J. F., Krotkov, N. A., Gille, J. C., Pickering, K. E., and Livesey, N.: Satellite observations of changes in air quality during the 2008 Beijing Olympics and Paralympics, Geophysical Research Letters, 36, https://doi.org/10.1029/2009GL039236, 2009.

Wittrock, F., Oetjen, H., Richter, A., Fietkau, S., Medeke, T., Rozanov, A., and Burrows, J. P.: MAX-DOAS measurements of atmospheric trace gases in Ny-Alesund - Radiative transfer studies and their application, Atmospheric Chemistry and Physics, 4, 955–966, https://doi.org/10.5194/acp-4-955-2004, 2004.

Wu, F. C., Xie, P. H., Li, A., Chan, K. L., Hartl, A., Wang, Y., Si, F. Q., Zeng, Y., Qin, M., Xu, J., Liu, J. G., Liu, W. Q., and Wenig, M.: Observations of SO_2 and NO_2 by mobile DOAS in the Guangzhou eastern area during the Asian Games 2010, Atmospheric Measurement Techniques, 6, 2277–2292, https://doi.org/10.5194/amt-6-2277-2013, 2013.

Zhang, J., Wang, S., Guo, Y., Zhang, R., Qin, X., Huang, K., Wang, D., Fu, Q., Wang, J., and Zhou, B.: Aerosol vertical profile retrieved from ground-based MAX-DOAS observation and characteristic distribution during wintertime in Shanghai, China, Atmospheric Environment, 192, 193 – 205, https://doi.org/https://doi.org/10.1016/j.atmosenv.2018.08.051, 2018.

Zhang, Q., Streets, D. G., He, K., Wang, Y., Richter, A., Burrows, J. P., Uno, I., Jang, C. J., Chen, D., Yao, Z., and Lei, Y.: NO_x emission trends for China, 1995-2004: The view from the ground and the view from space, Journal of Geophysical Research: Atmospheres, 112, https://doi.org/10.1029/2007JD008684, 2007.

Zhang, R., Tie, X., and Bond, D. W.: Impacts of anthropogenic and natural NO_x sources over the U.S. on tropospheric chemistry, Proceedings of the National Academy of Sciences, 100, 1505–1509, https://doi.org/10.1073/pnas.252763799, 2003.

Zhao, B., Wang, S. X., Liu, H., Xu, J. Y., Fu, K., Klimont, Z., Hao, J. M., He, K. B., Cofala, J., and Amann, M.: NO_x emissions in China: historical trends and future perspectives, Atmospheric Chemistry and Physics, 13, 9869–9897, https://doi.org/10.5194/acp-13-9869-2013, 2013.